M. Bosio, S Labò, P Riva, A Belleri. 2023. "Seismic risk and finite element modelling influence of an existing one-storey precast industrial building". Journal of Earthquake Engineering

Publisher's version at: https://doi.org/10.1080/13632469.2022.2162631

Seismic risk and finite element modelling influence of an existing one-storey precast industrial building

Marco Bosio[1], Simone Labò[1], Paolo Riva[1], Andrea Belleri[1*]

[1] Department of Engineering and Applied Sciences, University of Bergamo, Viale Marconi 5, Dalmine, Italy

[*] corresponding author: andrea.belleri@unibg.it

Abstract

Precast structures are widely used in Southern Europe particularly for industrial buildings. Most of such buildings have been built before the enforcement of modern anti-seismic regulations showing a poor performance during past major earthquakes. Focusing on existing one-storey precast industrial buildings, the paper investigates the influence of modelling choices on the risk assessment, direct losses, and required structure retrofit time. RC forks, cladding panels, and elements connections were specifically considered. A precast industrial building with structural details compatibles with 1980s Italian regulations was selected and analysed. In general, the failure was associated with the collapse of roof elements.

Keywords: precast structures; industrial buildings; seismic risk; beam-column connections; friction connections

1. Introduction

The interest in the seismic risk assessment of existing structures is constantly growing especially in countries such as Italy in which a great share of the building stock was conceived without appropriately accounting for seismic actions: these buildings were designed before the introduction of modern seismic regulations or in areas not considered as seismic at the time of construction and, consequently, adequate anti-seismic details were not prescribed. Through the seismic risk assessment, the buildings' conditions may be evaluated to promote appropriate retrofit interventions if the safety level is not appropriate.

In this article, which focuses on industrial reinforced concrete (RC) precast structures, the seismic performance of a case study building designed for 1980s Italian building regulations for three different sites with increasing seismicity is investigated accounting for the influence of finite element modelling strategies on the seismic risk. The focus on industrial precast structures is dictated by the poor performance of existing buildings in past earthquakes, such as the seismic sequence that hit the Emilia-Romagna region (Italy) in 2012, where several one-storey industrial buildings were severely damaged and experienced local roof collapses due to the poor performance of the roof connections and failure of the peripheral cladding system.

The considered structural typology is characterized by single-storey systems whose gravity and horizontal loading is taken by cantilever columns considered fix-connected to the foundation through socket connections or mechanical systems (Osanai et al. 1996; Dal Lago et al., 2016; Metelli et al., 2011; Belleri and Riva, 2012). The main beams are generally prestressed and supported to the columns through either dowel connections

(Clementi at al., 2016; Magliulo et al., 2014; Zoubek et al., 2015; Kremmyda et al., 2014) or simple bearing (Casotto et al., 2015; Demartino et al., 2018; Ercolino et al., 2016; Bosio et al. al., 2020; Labò et al., 2022); the latter is found for old buildings not designed for seismic actions, where friction was considered sufficient for the horizontal load transfer. The roof elements are generally made of long span precast double-tee or winged beams simply supported on the main girders and connected through mechanical systems or simple friction, for new or old buildings, respectively. An additional RC topping may exist or not to provide a roof diaphragm action.

The seismic design and assessment of such buildings may be carried out following both traditional and displacement-based approaches (Biondini and Toniolo, 2009; Biondini et al., 2010; Colombo et al., 2016; Belleri, 2017; Torquati et al., 2018; Belleri and Labò, 2021; Bosio et al., 2020; Sousa et al., 2020). Considering the modelling strategies in the case of new buildings, specific considerations on this structural typology can be found in Magliulo et al. (2018, 2021), Gajera et al. (2021), Bressanelli et al. (2019, 2021), Rodrigues et al. (2021), Zoubek et al. 2014, De Stefani and Scotta (2022). During past earthquakes, the main seismic vulnerabilities observed were related to the loss of support of beam and roof elements, to the failure of RC forks at the top of the columns, to the failure of dowel connections, to the overturning of RC cladding panels among others (Belleri et al., 2015; Bournas et al., 2014; Magliulo et al., 2014; Minghini et al., 2016; Nastri et al., 2017; Palanci et al., 2017; Savoia et al., 2012; Belleri et al., 2016; Belleri et al., 2017; Scotta et al., 2015; Toniolo and Colombo 2012; Menichini et al., 2020).

The results described in this article has been partly obtained during an Italian national project (i.e., RINTC-E, Iervolino et al. 2022; Bosio et al. 2022) aiming at assessing the seismic risk of existing structural typologies as a function of past building codes prescriptions. The focus of this paper is placed specifically on one of the precast buildings addressed in the project by additionally addressing the influence of the modelling strategies of typical seismic vulnerabilities and including the assessment of direct losses and required retrofit time.

An existing precast industrial building with structural details for non-seismic regions was selected and considered located in three sites with increasing seismic intensity: the structural details of the case study were adapted to the code prescriptions of 1980s (D.M. 108/86, 1986) for the sites of Milano, Napoli and L'Aquila considered at that time as non-seismic, medium, and high-intensity seismic areas, respectively. The available structural details were taken directly from an existing building not designed for seismic actions, therefore, such details were considered for the building located in Milano, while a re-design was carried out for the sites of Napoli and L'Aquila.

Non-linear dynamic analyses at ten intensity levels accounting for record-to-record variability were performed for each considered site and two performance levels were considered: Usability Preventing Damage (UPD) and Global Collapse (GC). Global Collapse refers to the collapse of a main element of the structure (column, beam or roof element), while Usability Preventing Damage refers to the RC element cracking limit state, the beam and roof elements sliding, and the precast cladding failure. The results allow comparing the influence of various modelling strategies for the existing elements and their connections. In general, it has been observed that the recorded failure was mainly associated with the local collapse of roof elements both in the case of friction and mechanical connections, while the out-of-plane failure of the main girders was not recorded. In addition, the complete modelling of the cladding system (i.e., horizontally and vertically spanning RC cladding panels) was found to significantly influence the UPD performance level leading to an important increase of the estimated economic losses and the related repairing and inactivity time of the building.

2. Reference building codes

The reference building code enforced at the time of construction (i.e., the 1980s) is DM 108/86 which classified the Italian territory into three seismic categories plus a fourth one without classification. To derive the seismic actions, the building code introduced a response coefficient (*R*) defined as a function of the fundamental period (T_0), and a seismic protection coefficient (*I*); the latter equal to 1.4 in the case of buildings of primary importance (e.g., civil protection), 1.2 for buildings classified for significant risk, and 1.0 for all other categories. It is worth noting that *R* is a reduction coefficient used to build the design spectrum for buildings with T_0 higher than 0.8 s:

$$\begin{aligned} &T_0 > 0.8s \qquad R = \frac{0.862}{T_0^{2/3}} \\ &T_0 \le 0.8s \qquad R = 1 \end{aligned} \tag{1}$$

In the case of framed buildings, T_0 could be estimated as:

$$T_0 = 0.1 \cdot \frac{H}{\sqrt{B}} \tag{2}$$

where *H* and *B* are the height and the smallest in-plan dimension of the building expressed in meters. Given *I* and *R*, and the weight of the building (*W*), the horizontal and vertical static forces (F_h, F_v) to be applied to the structure could be derived as:

$$\begin{aligned} &F_h = C \cdot R \cdot I \cdot W \\ &F_v = m \cdot R \cdot I \cdot W \end{aligned} \tag{3}$$

where *m* is an amplification coefficient for vertical forces (typically set equal to 2) and $C = \frac{S-2}{100}$ is the seismic intensity coefficient expressed as a function of the seismicity degree (*S*) defined for each seismic region. Therefore, for *R* and *I* equal to 1, the horizontal seismic action could be considered as a percentage of the structural weight: 4% for sites falling in "seismic category III", 7% for sites falling in "seismic category II", and, in the most severe case, 10% for sites falling in "seismic category I". Generally, the seismic actions could be distributed along the building height proportionally to the mass distribution. As for the vertical component of the seismic action, this could be neglected except in the cases of horizontal members with span greater than 20 m, pushing-type structures, and overhangs. Considering precast roofs, mechanical connections between the various elements were required only for buildings in seismic regions. Moreover, CNR 10025/84, which transposed the indication given by DM 108/86 and collected the "*prefabrication and prefabricated structures*" technical standards, did not recommend simple friction support between structural elements. As for the connection of the structural elements (e.g., beam-column connections), CNR 10025/84 prescribed that the RC forks at the top of the columns must be able to carry a bending moment (*M*) equal to:

$$M = V \cdot \left(L/_{300} \right) \quad (4)$$

where V is the shear force and L is the beam length. A minimum of 9 cm thickness in the lower portion and 7 cm in the upper portion of the fork are also prescribed. The maximum height of a RC fork could not exceed 8 times its average thickness, while the width must be equal at least to the length of the bearing length of the beam. A minimum steel reinforcement ratio of 1.5% should be guaranteed. In the case of simple friction support, the beam stability must be guaranteed even in the cases of construction-related imperfections, impacts, or wind loads.

CNR 10025/84 also deals with non-structural elements such as infill panels and non-load-bearing panels. As for the infills, an adequate connection to the structure must be guaranteed. In the case of horizontally spanning cladding panels, they must be suitably anchored to the vertical structural elements; in the case of vertically spanning cladding panels, they require connections to the ground and to the top beams. The anchoring must be applied in the RC core at a distance greater than 4 cm from the edge of the element and 2 cm from the reinforcing bars. Finally, for non-load-bearing panels, connections must not affect the structural stiffness and they should ensure a ductile behaviour.

3. Reference case study

The reference case study resembles the structural details of a real precast industrial building built in Emilia-Romagna (Italy) in the 1980s; the structural drawings of the building were used to emulate the design practice of the time. It is worth noting that Emilia Romagna was not considered as a seismic area at that time, therefore the same structural details were used for the site of Milano while some variations were made for the buildings considered located in Napoli and L'Aquila to fulfil the building code prescription for seismic regions.

The building has a 20 m x 42 m rectangular plan; the bearing structure consists of eight one-direction frames in the longitudinal direction equally spaced with a total height equal to 9.0 m (**Figure 1**). The main girders are double-tapered prestressed RC beams which support double-tee roof elements. The beams are housed in RC forks at the top of the columns, ensuring stability and providing appropriate retention against out-of-plane overturning of the beam in the assembly phases. The cladding system is made of precast RC panels. Along the longitudinal direction, 4 levels of horizontally spanning panels are present with ribbon windows between the 3rd and the 4th row. Such panels are connected to the columns by 2 bearing connections at the bottom of the panel (a bearing bolt ϕ24 laying on a steel bracket) and 2 retaining hammer-head anchor bolts at the top (ϕ16 and anchor channel 40 x 2.5 mm) (Belleri et al. 2016, Belleri et al. 2018). In the transverse direction, vertically spanning cladding panels are present and anchored to the grade beam by a L-shape steel plate and to the top beam by a hammer-head stripe connection (anchor channel 40x2.5 mm) (Zoubek et al. 2016, Belleri et al. 2017).

Since the design of the original building was governed by gravity loads, no specific details were provided for the roof element connections which are just lying on the main girders, thus relying only on friction for the transmission of horizontal forces. It is worth noting that it was common to interpose a neoprene pad between the surfaces to ensure uniform distribution of the vertical stress.

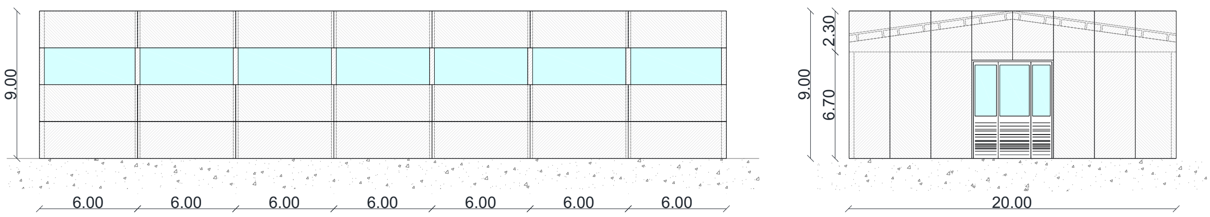

Figure 1 Longitudinal and transverse view of the reference case. Note: measures are in meters.

Figure 2 shows the columns structural details. The columns of the case studies located in Milano and Napoli have the same cross-sections (50 cm x 40 cm) and placed with the higher inertia in the transverse direction (**Figure 2b**). As for the case study located in L'Aquila, a 50 cm x 50 cm cross-section is reported (**Figure 2c**). In both the cases, 2 ϕ14 longitudinal rebars are placed in the first 3.00 m in addition to 4+4 ϕ14 mm longitudinal rebars along the whole column height. Stirrups ϕ8 mm@200 mm were considered. The cross-section highlights the common practice of the time to use small diameter reinforcing bars grouped at the corners. As for the RC fork at the column top, the reinforcement is made of 6 ϕ8 mm U-shaped longitudinal bars anchored in the column, and stirrups ϕ5 mm @ 200 mm. The small cross-section thickness combined with the multiple reinforcement layers suggests a small concrete cover which could lead to durability issues.

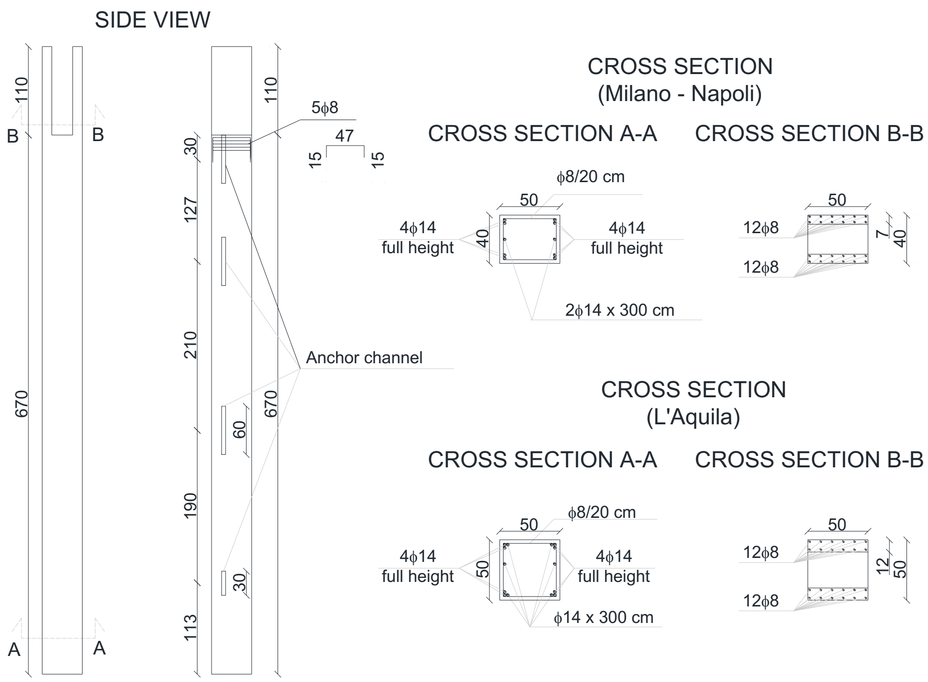

Figure 2 Details and cross-section of the columns. Note: measures are in cm.

Figure 3 shows the roof elements. **Figure 3a** depicts the double-tapered beam which has an almost rectangular cross-section at the support (to guarantee adequate shear capacity) and a slenderer I-section in the middle (to maximize the bending moment capacity). Simple friction beam-column connections were observed for the reference building; the same details were considered for the case study located in the Milano site (i.e. for a non-seismic region in the reference building code). To account for the code specifications (CNR 10025/84) in the case studies located in Napoli and L'Aquila sites (i.e. for seismic regions in the reference building code), 2 M24 dowels were introduced at the beam-column joint. **Figure 3b** shows the double-tee roof element which spans between two adjacent double-tapered beams. Eight double-tee roof elements are placed in each span.

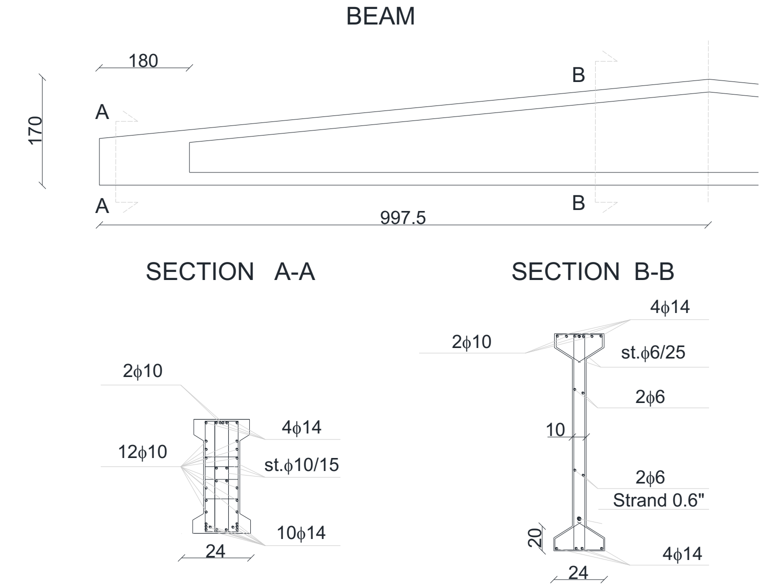

a)

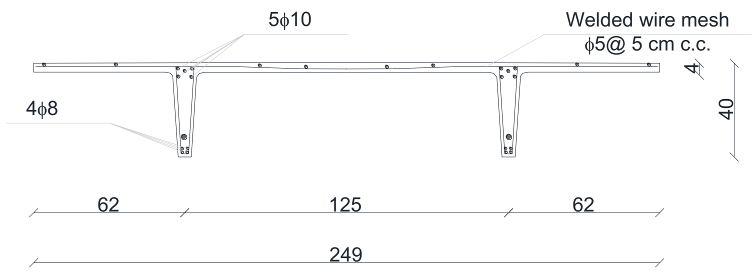

b)

Figure 3 Structural details of the roof system: a) double-tapered beam, and b) double-tee roof element. Note: measures are in cm.

Figure 4 shows the details of the beam-column and the beam-roof element connections. It is worth noting the presence of a mechanical connection (i.e., steel brackets) between the gutter beam and the main girder which inhibits the relative displacements of the roof elements along the main girder direction and transfers the wind actions acting on the cladding panels; at the same time, such connection improves the out-of-plane stability of the double-tapered beams. Above the main girders, an additional RC curb was cast between consecutive roof elements (**Figure 4b**).

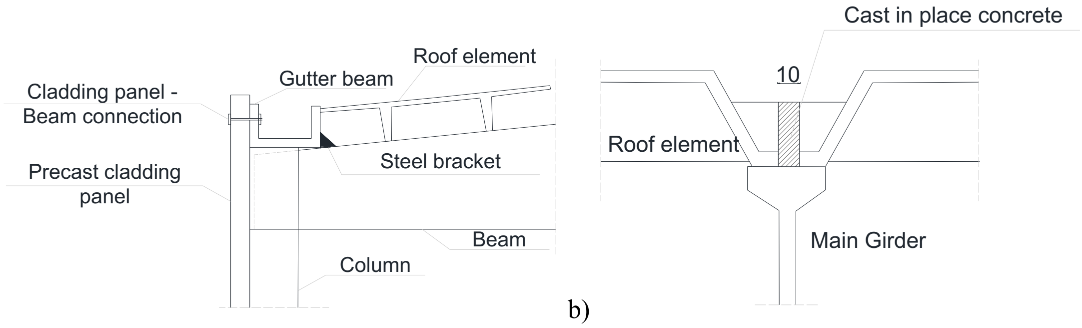

Figure 4 Structural scheme of the a) gutter beam to main girder connection and b) RC curbs in between the roof elements.

Such structural details were directly adopted for the building considered located in Milano, i.e. for a non-seismic region according to DM 108/86. For the buildings in Napoli and L'Aquila, which were classified as seismic regions at that time, a re-design was carried out following the DM 108/86 and CNR 10025/84 prescriptions and guidelines. As for the columns, the same cross-section AA was sufficient for the case of Napoli because for this site the seismic actions were lower than the wind actions, while the cross-section BB was obtained from the re-design of the columns for L'Aquila building: 6 ϕ14 longitudinal rebars are placed in the first 3.00 m in addition to 4+4 ϕ14 mm longitudinal rebars along the whole column height. Stirrups ϕ8 mm @ 200 mm were considered. Mechanical connections were placed between the roof elements and the supporting beams by means of metal brackets anchored by ϕ10 mm and ϕ12 mm dowels having a shear capacity of 10.4 kN and 25.6 kN, for the cases of Napoli and L'Aquila, respectively (Dal Lago et al., 2017). As for the RC forks, an increase of the cross-section was required to meet the minimum thickness as addressed in CNR 10025/84: the thickness of the RC fork was increased from 6 cm to 10 cm, and from 6 cm to 12 cm for the cases of Napoli and L'Aquila, respectively.

To summarize, no changes to the original structural details were required for the building located in Milano; for the building located in Napoli (low seismicity according to DM 108/86), the minimum standards and design practices were enough to satisfy the load demand; for the building located in L'Aquila, the main structural elements had to be re-designed to carry the seismic loads. The cases of Napoli and L'Aquila required connections for the roof elements (DM 108/86), being Napoli and L'Aquila classified as seismic sites. **Table 1** shows a summary of the construction details. Regarding the mechanical characteristics of the construction materials, the rebars yield and the concrete strength were taken equal to 470MPa and 43MPa, in accordance with the documentation of the reference building. Class 6.5 bolts (i.e. yield stress equal to 300 MPa) were considered for the mechanical connections.

Table 1. Main construction details for each considered site.

	Milano	Napoli	L'Aquila
Column cross-section	50 cm x 40 cm	50 cm x 40 cm	50 cm x 50 cm
Column longitudinal rebars	12 ϕ 14	12 ϕ 14	14 ϕ 14
Column stirrups	ϕ 8 @ 20cm	ϕ 8 at @ 20cm	ϕ 8 @ 20cm
Beam-column connection	RC fork 6 cm x 50 cm 6+6 ϕ 8 (U-shaped)	RC fork 10 cm x 50 cm 6+6 ϕ 8 (U-shaped)	RC fork 12 cm x 50 cm 6+6 ϕ 8 (U-shaped)
Roof-element-beam connection	Friction	Dowel connection (ϕ10)	Dowel connection (ϕ12)
Horizontally spanning cladding panel connection	Top connection: Hammer-head bolt ϕ16 - Anchor channel 40x2.5 mm		
Horizontally spanning cladding panel connection	Bottom connection: Bearing bolt ϕ24 on steel bracket		
Vertically spanning cladding panel connection	Top connection: Hammer-head stripe bolt - Anchor channel 40x2.5 mm		
Vertically spanning cladding panel connection	Bottom connection: L-shape steel plate		

4. Finite Element Model

The Finite Element (FE) model of the considered buildings was developed with the software OpenSees (McKenna and Fenves, 2001). In the FE model definition the focus was made on: a) the plastic hinge at the base of the column, b) the plastic hinge at the base of the RC forks, c) the stabilizing moment due to gravity load acting on the double-tapered beam, d) the contact between the beam and the RC fork to account for beam overturning actions, e) the hysteretic model of the connections of the roof elements, f) the friction connections, g) the cladding system. The FE modelling strategies for the aforementioned quantities and elements are reported in the following.

The columns were modelled with beam elements fixed at the base and subdivided into four sub-elements to allow for connections to the cladding panels. No assessment of the foundation capacity was carried out herein. The Modified Ibarra-Medina-Krawinkler Deterioration Model with Peak-Oriented Hysteretic Response ("ModIMKPeakOriented" Material) (Ibarra et al., 2005) shown in **Figure 5**a was considered for the plastic hinge in terms of moment-rotation response; a zero-length element was adopted. Analogously for the RC fork plastic hinge, where a zero-length element was placed at the base of each element of the fork. The main parameters of the hysteretic system are reported in **Table 2**.

Table 2. Plastic hinge main parameters for the inflected elements.
Note: K_0 is the initial stiffness; K_1/K_0 is the strain hardening ratio; M_y and F_y are the moment and force at yielding; ϑ_p and d_p are the pre-capping rotation and displacement; ϑ_{pc} and d_{pc} are the post-capping rotation and displacement; ϑ_u and d_u are the ultimate rotation and displacement capacity.

Structural element	**K_0 [kNm/rad]**	**K_1/ K_0 [#]**	**M_y [kNm]**	**ϑ_p [rad]**	**ϑ_{pc} [rad]**	**ϑ_u [rad]**
Column 40 cm x 50 cm Direction of lower inertia	32900	0.08	203.9	0.0151	0.0358	0.2
Column 40 cm x 50 cm Direction of higher inertia	43100	0.07	262.7	0.0174	0.0432	0.2
Column 50 cm x 50 cm	45200	0.07	289.45	0.0186	0.453	0.2
RC Fork 7 cm thick	2222	0.3	21.78	0.0066	0.018	0.2

RC Fork 10 cm thick	4018	0.3	37.12	0.066	0.018	0.2
RC Fork 12 cm thick	5686	0.3	52.88	0.0067	0.018	0.2
Connection	**K_0 [kN/m]**	**K_1/ K_0 [#]**	**F_y [kN]**	**d_p [m]**	**d_{pc} [m]**	**d_u [m]**
Beam-column dowel	105000	0	159.39	0.012	0.02	0.036

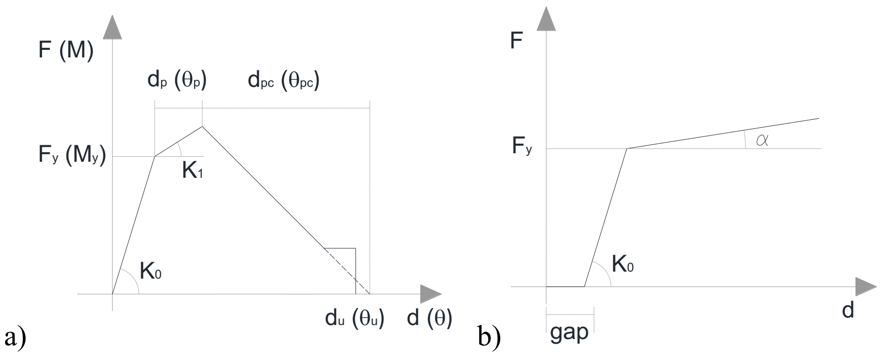

Figure 5 Hysteretic model: a) Modified Ibarra-Medina-Krawinkler Deterioration Model with Peak-Oriented Hysteretic Response, and b) Steel01 (with α=0), Elastic-Perfectly Plastic Material (with α=0, and gap=0), and Elastic-Perfectly Plastic Gap Material (with α=0).

Regarding the RC fork model, two strategies were investigated (**Figure 6**) to account for the interaction with the out-of-plane movements of the main girder. The first model exploited the out-of-plane rocking motion of the main girder through horizontal rigid elements at the base of the girder connected to compression-only springs. The second model considered a plastic hinge at the base of the girder with a flexural capacity expressed as a function of the stabilizing moment associated with the effective vertical loads acting on the girder due to the supported roof elements. However, in dynamic conditions, the value of this moment is constantly changing because of the vertical component of the earthquake and because the model adopted accounts for the removal of the elements when a limit condition is exceeded. In fact, in the case of a roof element removal, a non-symmetrical reduction of the vertical loads occurs, thus resulting in a non-symmetrical change of the overturning capacity. To account for this aspect, a specific calculation code was introduced in the FE script to calculate, at each step of the analysis, the nonlinear properties of the plastic hinges associated with the overturning moment capacity of the girder. In both models, two compression-only elements were placed at the top of the girder to engage the flexural capacity of the RC forks. Such elements were provided with a 1 cm gap to account for the gap associated with tolerance issues. Among the two models, the second option was the more stable in computational terms and therefore chosen in the analyses: in fact, in the first option, a net uplift load at the rocking interface may arise because of a combination of the vertical component of the ground motion and the forces arising as a consequence of the instant vertical load removal of the roof elements. Such condition led to analysis' non convergence.

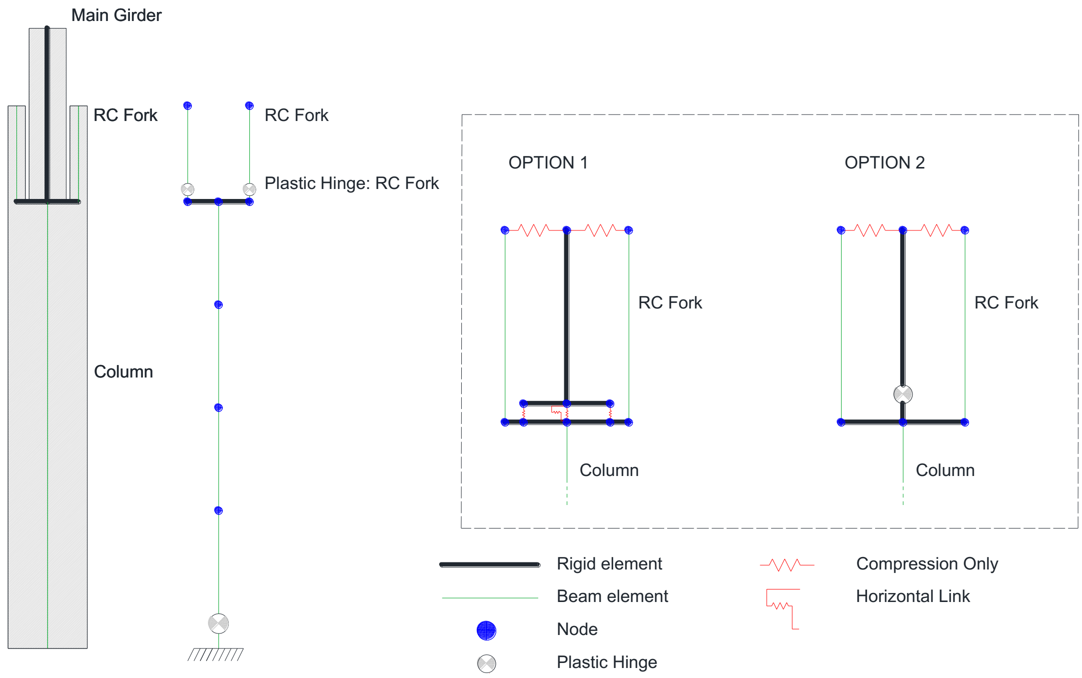

Figure 6 Beam-fork connection to capture the out-of-plane rocking motion of the main girder.

Regarding the double-tapered beam, rigid elements were introduced as shown in **Figure 7a** to place the bearing connections of the double-tee roof elements in their actual position. The out-of-plane movements at the girder ends were previously described. Regarding the in-plane movements, a friction connection was placed at the beam-column interface for the site of Milano, while dowel connections were considered for the other sites. In the first case, the neoprene-concrete interface was modelled by means of a “Flat Slider Bearing Element” with a friction coefficient (μ) equal to 0.13 (from Magliulo et al., 2011) and initial stiffness equal to 490 kN/m (i.e., transverse neoprene pad stiffness; Bosio et al. 2020). In the latter case, the “Modified Ibarra-Medina-Krawinkler Deterioration Model” with Peak-Oriented Hysteretic Response was considered for the plastic hinge definition in terms of load-displacement (Bressanelli et al. 2021).

Figure 7b shows a sketch of the roof element highlighting the subdivision into four elements and the position of the roof element-girder connections. As for the case of Milano, a simple friction connection between the double-tapered beam and the roof elements was introduced according with the same considerations followed to model the beam-column connection (Bosio et al. 2020). A 6 cm support mean length was considered following a normal distribution with a 1 cm standard deviation to account for the possible influence of tolerance issues. Three different models were investigated to consider the interaction between the roof elements and between the roof elements and the adjacent structural elements. In the first model, the roof elements were free to move in all directions, without accounting for possible elements contacts. In the second model, the interaction between adjacent roof elements was accounted for, and, in the third model, the interaction between roof elements and the RC curbs or the gutter beams was introduced by means of an “Elastic No Tension” behaviour through “Two Node Link” elements. For the case located in Milano, an additional model was also considered by adding a rigid diaphragm behaviour of the roof, as in the case of a cast in place RC topping layer. For the sites of Napoli and L’Aquila, mechanical connections were additionally introduced to satisfy the building code prescriptions (DM 108/86). The mechanical connections were modelled by means of "Zero-Length" elements in parallel with the friction connection. Each mechanical connection was modelled with an elastoplastic (Elastic-Perfectly Plastic Material) hysteresis and removed after reaching its capacity (10.4 kN and 25.6 kN for Napoli and L'Aquila, respectively).

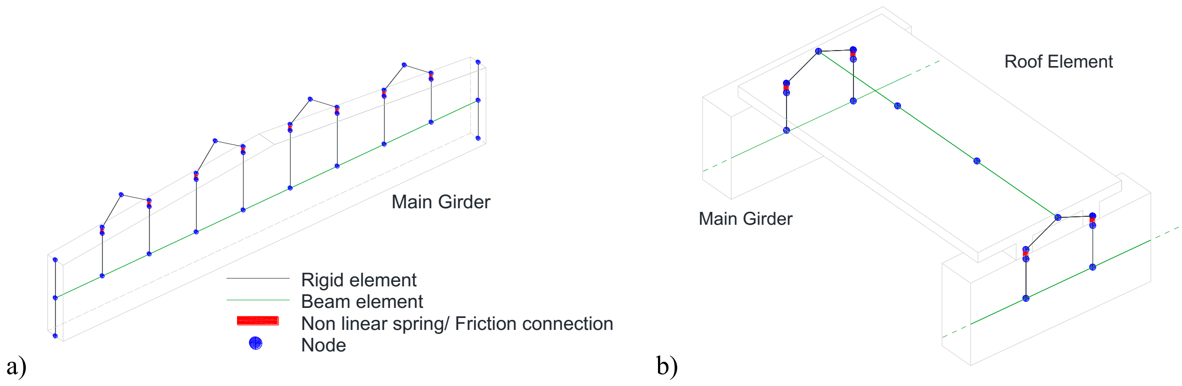

Figure 7 Modelling scheme of the roof (a) main girder and (b) roof elements.

Considering the cladding panels, they were modelled both in terms of lumped masses at the connection nodes with the columns and the beams (for the horizontal and vertical cladding panels, respectively) or by completely modelling the panel and its connections. In the latter case, a subdivision of the cladding panel element into three sub-elements was carried out and rigid elements perpendicular to the panel longitudinal axis were placed at each end of the panel to reach the actual position of the connections (**Figure 8**). As for the cladding panels connections, nonlinear springs were introduced. The hysteretic models shown in **Figure 5b** were adopted and the parameters involved are summarized in **Table 3**.

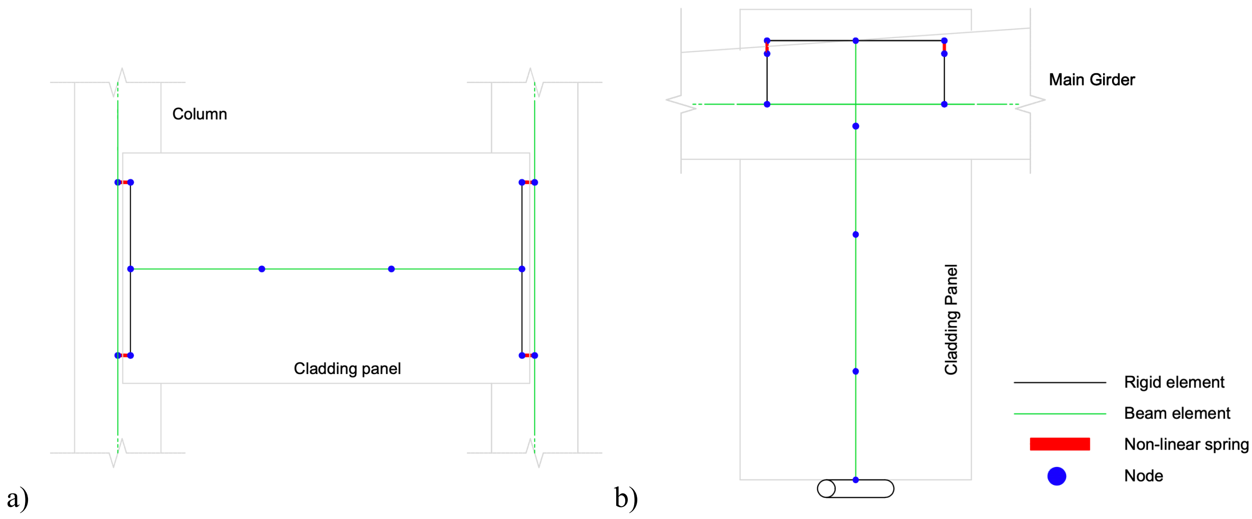

Figure 8 Modelling scheme of (a) horizontally and (b) vertically spanning cladding panels.

Although the devices typically used to connect the panels to the structural elements are different for vertically and horizontally spanning cladding panels, their performance during an earthquake is very similar and it could be represented by a set of nonlinear springs acting in parallel. When both the top retaining connections reach their ultimate capacity, the mass of the panel was removed from the FE model.

Table 3. Hysteretic models shown in **Figure 5**b adopted for the nonlinear springs adopted for each cladding panel connection. Note: K_0 is the initial stiffness of the connection; F_y is the yielding force of each component of the connection; Gap is the initial gap considered in the hysteretic model. Elastic PP, Elastic PPgap and Steel01 refer to the OpenSees materials considered.

	Connection	Direction	OpenSees material	K_0 [kN/m]	F_y [kN]	Gap [m]	Hardening ratio
Vertical panel	In-plane (upper conn.)	symmetric for positive and negative displacements	Elastic PPgap	571	1.33	0.035	-
			Elastic PPgap	21	13	0.037	-
	Out-of-plane (upper conn.)	approaching the support	Elastic PP	5000000	40	-	-
		away from the support	Elastic PPgap	25000	28	0.000008	-
Horizontal panel	In-plane (upper conn.)	symmetric for positive and negative displacements	Elastic PPgap	666	1.33	0.02	-
			Elastic PPgap	32	13	0.022	-
	Out-of-plane (upper conn.)	approaching the support	Elastic PP	5000000	40	-	-
		away from the support	Elastic PPgap	25000	28	0.00012	-
	In-plane (bottom conn.)	symmetric for positive and negative displacements	Elastic PPgap	10000	100	0.05	-
	Out-of-plane (bottom conn.)	approaching the support	Elastic PP	5000000	40	-	-
		away from the support	Steel01	1000	3	-	0.002

It is worth noting that the model allowed the element removal, through the “Remove” command, when a limit condition was exceeded. The element removal was applied to:

- vertically and horizontally spanning cladding panels: when the connections avoiding overturning failed (for both the cases in which they are modelled completely or through lumped masses. Both cases consider the contribution of torsion in the panels: Scotta et al. 2015 and Belleri et al. 2018).
- any mechanical connection: after reaching its ultimate capacity.
- roof elements: when the relative sliding between the roof element and the supporting beam is greater than the available bearing length.
- beam elements: when the friction sliding along its longitudinal axis is greater than the available bearing length or when the overturning around its longitudinal axis occurred.
- RC fork and columns: when the ultimate rotation was exceeded.

First the connection was removed once its ultimate capacity was reached, and then, when the ultimate condition of the structural element was verified (such as the loss of support of the main beams or of the roof element), the considered element was removed from the analysis. Regarding the point mass models of the cladding panels, the masses corresponding to a cladding panel were removed after reaching the panel ultimate in-plane and out-of-plane capacity. The in-plane capacity was inferred at the connection level from the horizontal relative displacements between the column points corresponding to the top and bottom cladding connections (Belleri et al. 2016); analogously for vertically spanning panels. The out-of-plane capacity was inferred at the connection level from the out-of-plane accelerations, i.e. assessing out-of-plane inertia loads, in the retaining connections and from the torsional motion of the panel assessed from the out-of-plane displacements of the points corresponding to the cladding connections, as reported in Scotta et al. 2015 and Belleri et al. 2018.

5. Influence of the modelling assumptions

For sake of brevity, an identification code was assigned to each of the considered FE model: the first letter represents the site (i.e., M=Milano, N=Napoli, A=L'Aquila), while the following number refers to the model number. The developed FE models are:

- M1: building in Milano; roof elements connected to the beam by neoprene-concrete simple friction; the sliding between beam and columns is not considered.
- M2: building in Milano; the modelling of the relative contact between the roof elements was added with respect to M1; the sliding between beam and columns is not considered.
- M3: building in Milano; modelling of the relative contact between the roof elements and the gutter beam and RC curbs at the top of the main girders was added with respect to M2; the sliding between beam and columns is not considered.
- M4: building in Milano; rigid diaphragm behaviour; friction sliding between the beam and the column.
- N1: building in Napoli; roof elements and beam-column mechanical connections modelled.
- A1: building in L'Aquila; roof elements and beam-column mechanical connections modelled.

In addition, a "C" label between the site letter and the model number identifies the models in which the panels are completely modelled, otherwise the cladding panels are just considered as lumped masses at the panel-to-structure connections. It is worth noting that the cladding panels were not completely modelled for the case M1 since it was considered a preliminary simplified model.

Table 4 provides a list of the main vulnerabilities of the structure and the related damage considered for the Usability Preventing Damage (UPD) and Global Collapse (GC) performance levels.

Table 4. Performance levels for the main vulnerability identified.

	UPD	**GC**
Column plastic hinge	Yielding rotation	Rotation capacity
Roof element-beam dowel connection	Failure of the connection	Loss of support
Roof element-beam friction connection	10% sliding compared to available seating length	Loss of support
Horizontally spanning cladding panels	UPD_1 – yielding of the connection UPD_2 – panel's collapse	-
Vertically spanning cladding panels	UPD_1 – yielding of the connection UPD_2 – panel's collapse	-

Multi-stripe analyses were performed through non-linear dynamic analyses at ten intensity levels accounting for record-to-record variability; for each intensity level, 20 ground motion records were considered. The records were selected in accordance with the RINTC project (Iervolino et al. 2022; Iervolino et al. 2018) reflecting the following earthquake return periods: [10; 50; 100; 250; 500; 1000; 2500; 5000; 10000;100000] years. Table 5 reports the elastic spectral acceleration at the fundamental period of vibration of the building (T1 = 2s) corresponding to each return period for the considered sites (i.e. Milano, Napoli, and L'Aquila). A soil category C (CEN 2004) was considered. First, the influence of the FE modelling assumptions is assessed with respect to the failure rate of the various vulnerabilities reported in **Table 4**, then, a seismic loss assessment is conducted in terms of economic losses and repair time.

Table 5. Spectral acceleration ($S_a(T_1)$) corresponding to each return period.
Note: $S_a(T_1)$ expressed in g.

$S_a(T_1)$ [g]	Return periods [years]									
Site	**10**	**50**	**100**	**250**	**500**	**1’000**	**2’500**	**5’000**	**10’000**	**100’000**
Milano	0.004	0.008	0.012	0.017	0.023	0.031	0.040	0.052	0.071	0.114
Napoli	0.007	0.021	0.041	0.063	0.089	0.0119	0.155	0.195	0.256	0.384
L’Aquila	0.011	0.026	0.049	0.080	0.124	0.184	0.270	0.379	0.572	1.077

5.1 Collapse rate

Regarding the number of failure events associated with the vulnerabilities reported in **Table 4**, the results of the case of Milano are plotted and discussed first (**Figure 9**), then the cases of Napoli and L’Aquila are considered (**Figure 10**). In all cases, for each vulnerability reported in **Table 4**, the results are expressed in terms of the median demand-capacity ratio as a function of the intensity levels. The cases with and without the complete modelling of the cladding are also compared (left and right sides of **Figures 9-11**, respectively). The values of the UPD and GC performance levels for each vulnerability are indicated in **Figure 9** and **Figure 10** by means of grey and black horizontal continuous lines, respectively.

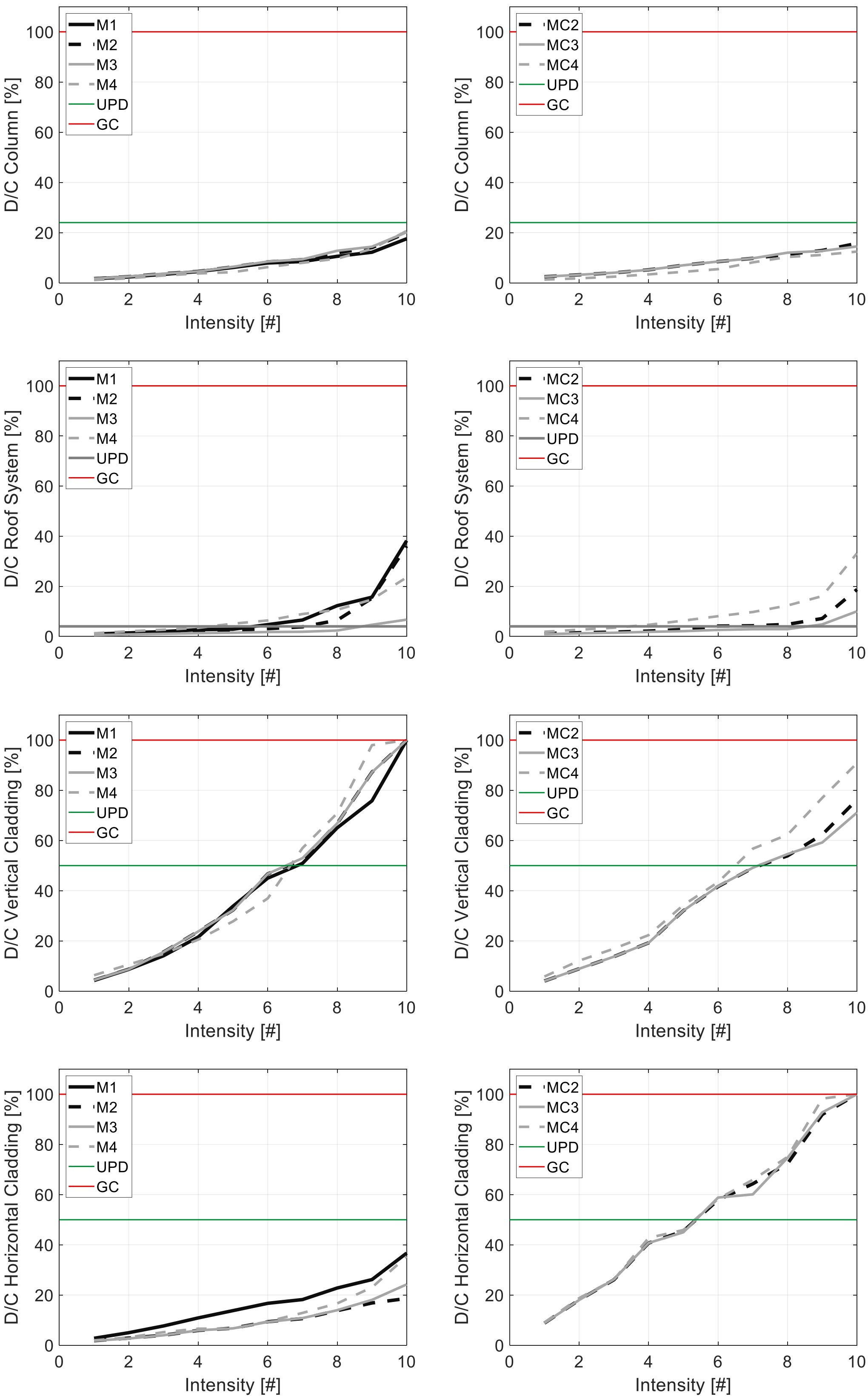

Figure 9 Demand-Capacity (D/C) ratio as a function of the intensity level for the case of Milano.
Note: Left side: cladding panels modelled as lumped masses. Right side: complete model of the cladding panels. The red and green horizontal lines represent the Global Collapse and Usability Preventing Damage performance levels, respectively.

The results in **Figure 9** highlight that the structural components did not show a significant vulnerability (demand-capacity ratio lower than 0.25) for the site of Milano. When the complete modelling of the cladding panels is introduced, a slight demand reduction in the columns was recorded, probably due to a light stiffening effect provided by the panel connections; no variations associated with the roof modelling were highlighted.
As for the roof system, the influence of its modelling is relevant: M1 and M2 present an increase in seismic vulnerability compared to M3, which means an increased vulnerability of the roof elements. In M4, with a diaphragm behaviour of the roof, the vulnerability increase compared to M3 is related to the friction sliding of the main girder. The complete modelling of the cladding panels leads to a reduction in the demand on the roof elements for MC2 and MC3 while a slight increase is observed for MC4.
As for the non-structural elements (i.e., vertically, and horizontally spanning cladding panels), it is observed that when they are modelled as lumped masses, the vertically spanning panels appear more vulnerable, although a complete modelling of the horizontally spanning panels leads to the opposite situation. With the complete modelling of the panels, the demand-capacity ratio of the horizontally spanning panels moves from 0.4 to 1. This increase depicts an early collapse of those panels thus highlighting the importance of such model type to appropriately capture the seismic vulnerability. The mass reduction obtained through the collapsed panels removal leads to a seismic demand reduction on the other structural elements such as columns. It is also worth noting that for the considered building, the seismic vulnerability of the horizontally spanning panels is also related to the in-plane stiffness of the roof; indeed, in the rigid diaphragm case (MC4) a higher demand is observed in the panels.
In general, it is observed that the complete modelling of the cladding panels leads to completely different results in terms of UPD but does not significantly affect the GC values. It is also observed that an excessive simplification in the roof modelling (i.e., neglecting the contact between adjacent elements) can lead to an overestimation of the identified vulnerabilities.
Figure 10 shows the results of the cases of Napoli and L'Aquila.

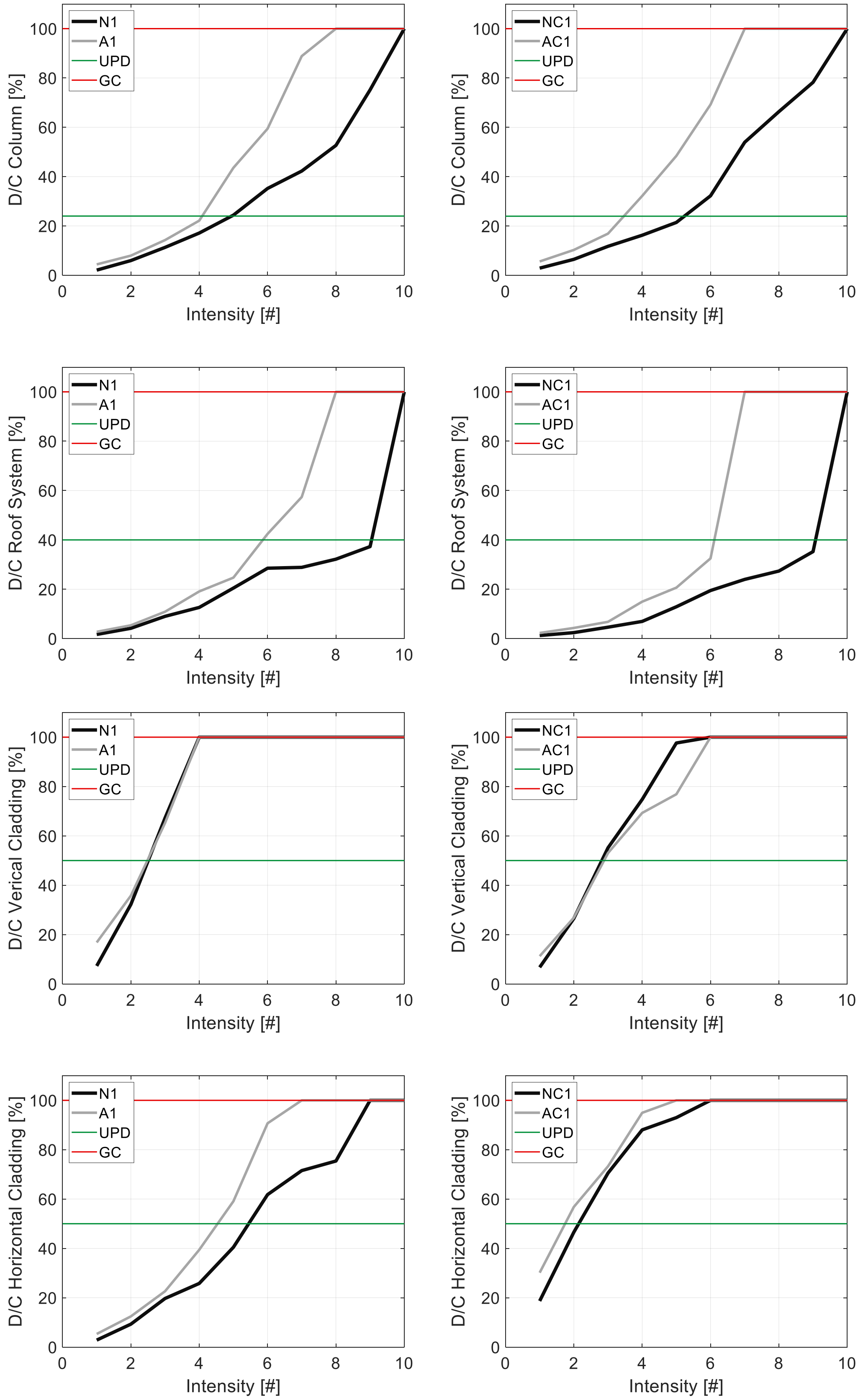

Figure 10 Demand-Capacity (D/C) ratio as a function of the intensity level for the cases of Napoli and L'Aquila. Left side: cladding panels modelled as lumped masses. Right side: complete model of the cladding panels.

For the cases of Napoli and L'Aquila, a significant increase in terms of vulnerability is observed both in terms of GC and UPD performance levels with respect to the case of Milano despite the buildings were re-designed according to the seismic code of the time. As for the columns, despite the structural details accounted for the seismic load (DM 108/86), the demand-capacity ratio exceeds the unit value. Except for the vulnerability of the vertically spanning cladding panels, in which marked differences cannot be found, the highest seismic vulnerabilities are associated with the case of L’Aquila due to its higher seismicity.

Similar considerations can be drawn for the roof elements. In this case, the reduction in demand following the complete modelling of the panels is much more evident. As for the cladding panels, as it was already observed in the case of Milano, the influence of the complete modelling of the panels affects the results: an increase in the vulnerability of the horizontally spanning panels for low intensity levels was recorded.

Despite the buildings were re-designed according with DM 108/86, several collapses were recorded. The number of collapses is summarized in **Figure 11** in terms of number of ground motions per intensity level in which the building experienced the collapse of the cladding panels or of structural elements. Both the cases of lumped mass and complete modelling of the cladding panels were considered.

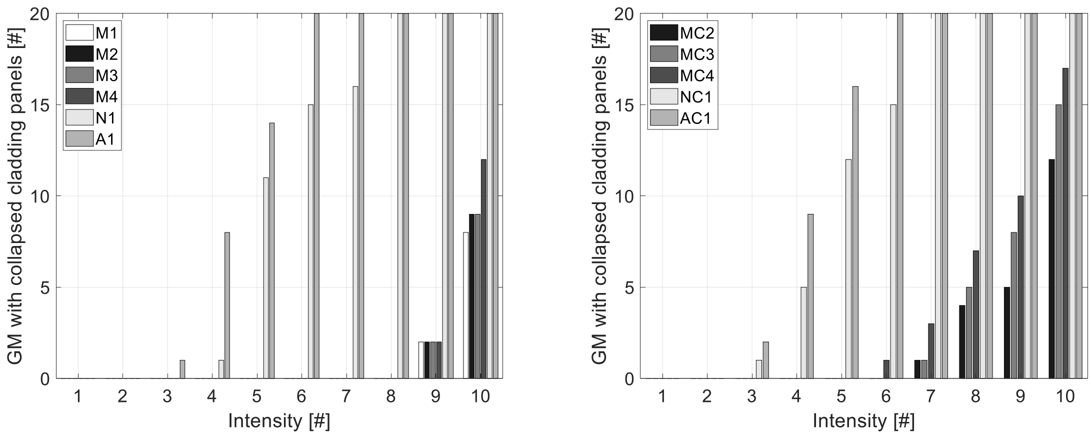

a)

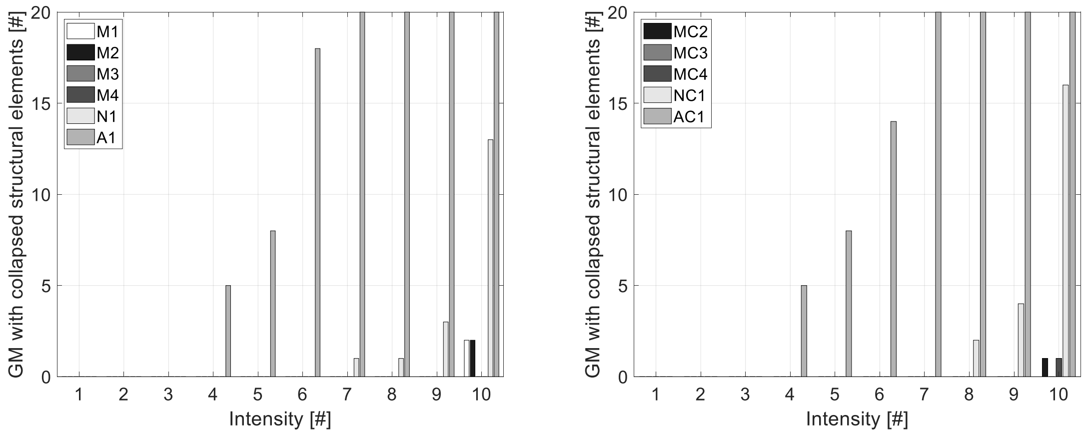

b)

Figure 11 Number of cases with collapses: a) collapse of cladding panels; b) collapse of structural elements.

As for the non-structural elements (cladding panels), their collapse is observed only for earthquake intensity levels equal to 9 and 10 in the case of Milano, and for intensity levels higher than 4 and 3 for the cases of Napoli and L’Aquila, respectively. The results showed that the complete modelling of these elements does not significantly affect the GC performance level while the UPD performance level experiences a decrease in the demand-capacity ratio. This clearly appears in the case of Milano where, without the complete modelling of the cladding panels, the collapse of the horizontal panels was not detected while a strong increase in the collapse of these elements occurs already for intermediate intensity levels (it moves from 9 to 6) with a complete modelling of the cladding system. No significant differences were recorded for the other cases of Napoli and L'Aquila; in the case of Napoli the minimum activation intensity level moves from 4 to 3 while no differences at all are shown for the case of L'Aquila. As for the GC performance level, the cladding panel modelling does not affect the results. No significant differences were recorded for the vertically spanning cladding panels.

Generally, the main vulnerability is associated with the roof elements; the column failure appears only for high intensity levels. In the considered cases, beam-column connections never reach their ultimate capacity.

In **Figure 12**, for the UPD performance level, the cladding modelling leads to a slight increase of the failure rate except for the cases M2 and N1 in which the failure rate decreases.

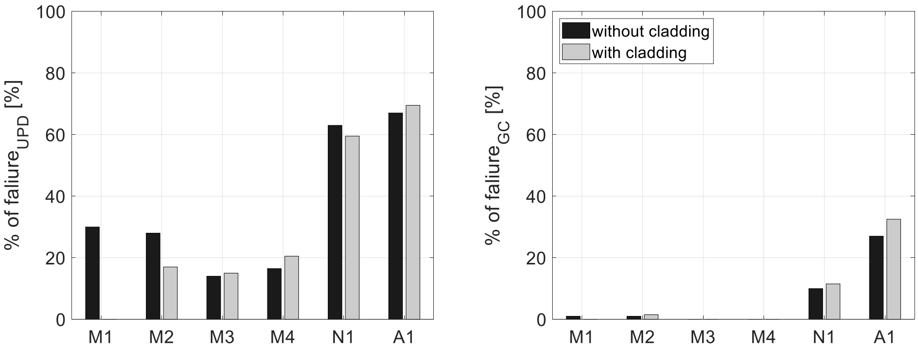

Figure 12 Rate of failure of each model: a) usability preventing damage (UPD) and b) global collapse (GC) performance levels with and without the cladding panels modelling.

5.2 Loss assessment

This section addresses the direct economic losses and the required recovery time in case of seismic events for the reference case study building. The evaluation of the direct losses is computed considering the main structural vulnerabilities for the reference case study, although it is worth to note that for industrial precast buildings the value of the content is often much higher than the value of the building itself. The procedure adopted moves directly from the PEER PBEE (FEMA P-58-3.1 2012) approach which allows calculating the expected losses following a four steps procedure: hazard analysis, structural analysis, damage analysis, cost analysis. The collapse hierarchy criterion addressed in Bosio et al. (2021) is considered to appropriately account for the peculiarities of this structural typology in which local collapses may arise; given the isostatic scheme of these structures, the collapse of a supporting element will eventually lead to the collapse of the supported elements thus significantly increasing the collapse probability and the loss values. For example, in the case of the failure of a main girder, all the roof elements bearing on such girder are considered collapsed; analogously, in the case of failure of a column, the supported girder and the related roof elements are considered collapsed.

The repair actions, repair costs and repair time at various damage levels of the structural and non-structural elements are reported in **Table 6**. The costs and the recovery time are estimated based on the Lombardia (Italy) price list for public works. It is worth noting that the recovery time accounts only for the retrofit actions, without considering the time required for the damage assessment, the retrofit design, post-earthquake grants application, authorizations and permissions. **Table 6** indicates the Damage State (DS) and the relative repair action for each element; the unit cost [€] and the time required to repair the damage occurring on one element [h] are reported for each repair action. The cost of a new building is herein approximately estimated as € 385000 for all the considered sites.

Table 6. Repair costs and repair time at the considered Damage States (DS).

Element	Damage state (DS) [Repair action]	Cost [€]	Time [h]
Column	DS1: Cracking [Epoxy resin injection]	77	0.5
	DS2: Concrete spalling [Replacement of concrete cover]	289	1
	DS3 Collapse [Column replacement]	2090	12
RC Fork	DS1 Cracking [Epoxy resin injection]	25	0.25
	DS2 Concrete spalling [Replacement of concrete cover]	59	0.5
	DS3 Collapse [Built a new fork]	252	2
Beam	DS3 Collapse [Beam replacement]	8628	8
Roof element	DS1 Small relative displacement [Replacement of the waterproofing system (25%)]	11	1
	DS2 medium relative displacement [Replacement of the waterproofing system (50%)]	23	2
	DS3 Connection yielding [Connection replacement]	34	0.5
	DS4 Connection collapse [Connection replacement]	48	1
	DS5 Loss of support [Roof element replacement]	801	4

Element	Damage state (DS) [Repair action]	Cost [€]	Time [h]
Horizontal cladding panel	DS1 Damage of joint sealant [Retrofit 50% of the joint sealant]	8	0.5
	DS2 Connection yielding [Connection replacement]	34	0.5
	DS3 Connection collapse [Connection replacement]	48	1
	DS4 Cladding panel collapse [Panel replacement]	826	4
Vertical cladding panel	DS1 Damage of joint sealant [Retrofit 50% of the joint sealant]	9	0.5
	DS2 Connection yielding [Connection replacement]	34	0.5
	DS3 Connection collapse [Connection replacement]	48	1
	DS4 Cladding panel collapse [Panel replacement]	1247	4

The total repair cost and time are calculated as the sum of the cost and time of each repair action times the number of the element requiring repair. It is important to note that, in case of significant damage (higher than 40 %-50 % of the cost of the new building), demolishing and rebuilding might be more economically convenient, however, this aspect is not herein accounted for, hence repair actions were always considered.

As for the total repair time, this was calculated based on an assumed time schedule prioritization which accounts also for some mandatory actions required to carry out the repair actions described in **Table 6**. Such mandatory actions are associated with post-earthquake safety measures, cleaning of the construction site, required element removal and waste disposal. These actions are scheduled at the beginning of the retrofit work. Following these operations, main and secondary operations are scheduled. The main operations are those whose interruption entails the construction work stop such as, for example, all the operations required to guarantee the safety against collapse due to gravity loads. The secondary operations are those related to the repair of non-structural damage, which does not compromise the stability of the building. As an example, when a new concrete casting is placed for the repair of a structural element, then, during the concrete curing, the following operations are scheduled and appropriately prioritized: concrete cover replacement and repair of the column and beam cracks by means of epoxy resins; beam-column connection replacement in terms of capacity; replacement of yielded and/or collapsed connections; concrete repair around the yielded and/or collapsed connections; repair of vertical and horizontal panel joints. To schedule such operations, the following priority value is assigned: columns, main girders, roof elements, horizontally and vertically spanning cladding panels. The prioritization has the purpose of identifying which operations need to be carried out first.

In general, for each operation, the repair times are assessed in advance and their compatibility with the various scheduled activities is verified; this means that the secondary actions can be scheduled in parallel to the main operations only if the available waiting-time is enough to allow for the operations completion; otherwise, secondary operations are postponed. An exploitable advantage of such strategy is the possibility of using the construction site downtime (e.g., the concrete curing time required) for other repairing operations thus optimizing the repair time.

The results of the loss analysis are reported in **Figure 13-15**. Referring to the case of Milano, **Figure 13** shows the ratio between the expected loss and the construction cost of the structure (**Figure 13a**) and the recovery time required to restore the building structure to its original conditions (**Figure 13b**). The expected losses are relatively low: for the intensity level 10 the maximum loss is almost 20% of the construction cost. It is worth noting that the complete modelling of the panels leads to an increase in the loss values which can be associated with the resulting higher demand on the horizontally spanning cladding panels. Similar considerations can be drawn for the recovery time. It is worth noting that the recovery time is also impacting the economic losses due to the inability to use the industrial building for almost 100 working days.

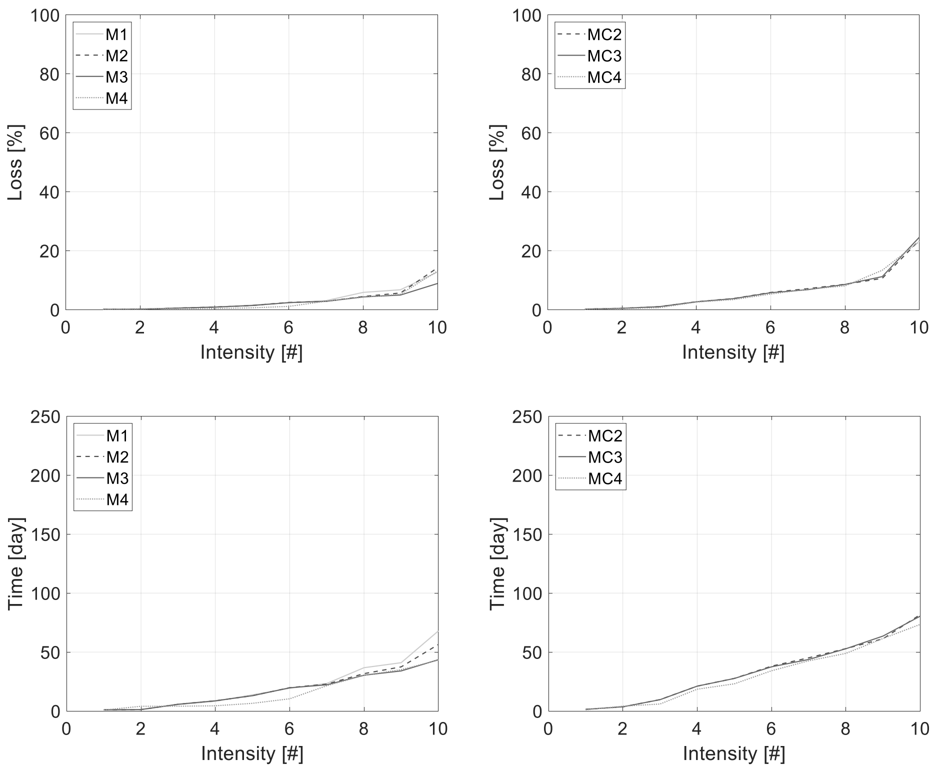

a)

b)

Figure 13 Normalized losses (a) and recovery time (b) for the case of Milano.

Figure 14 shows the results for the cases of Napoli and L'Aquila. A trend similar to the case of Milano is observed and higher loss values are recorded (more than 100 % of the construction cost and more than double recovery time with respect to the case of Milano). The losses and the recovery time increase significantly for high intensity levels; in **Figure 14a** losses increase very quickly for intensity levels higher than 6 and 8 for the cases of L'Aquila and Napoli, respectively, while in **Figure 14b** the recovery time shown a significant increase for intensity levels higher than 6. Accordingly, the losses and the recovery time are always greater in the case of L'Aquila than the case of Napoli due to the higher seismicity. It is worth remembering that the recovery time considers the time required to restore the building to the pre-earthquake conditions without considering the actual efficiency of such solution, therefore, without accounting for the possible economic advantage of demolishing and rebuilding the whole building. For such reason the loss ratio may be higher than 1.

Regarding the influence of the FE modelling strategy of the cladding panels, an increase of both the losses and the recovery time are observed, despite a higher computational burden for the higher intensities, thus remarking the importance of modelling these elements also for the assessment of repair costs and time.

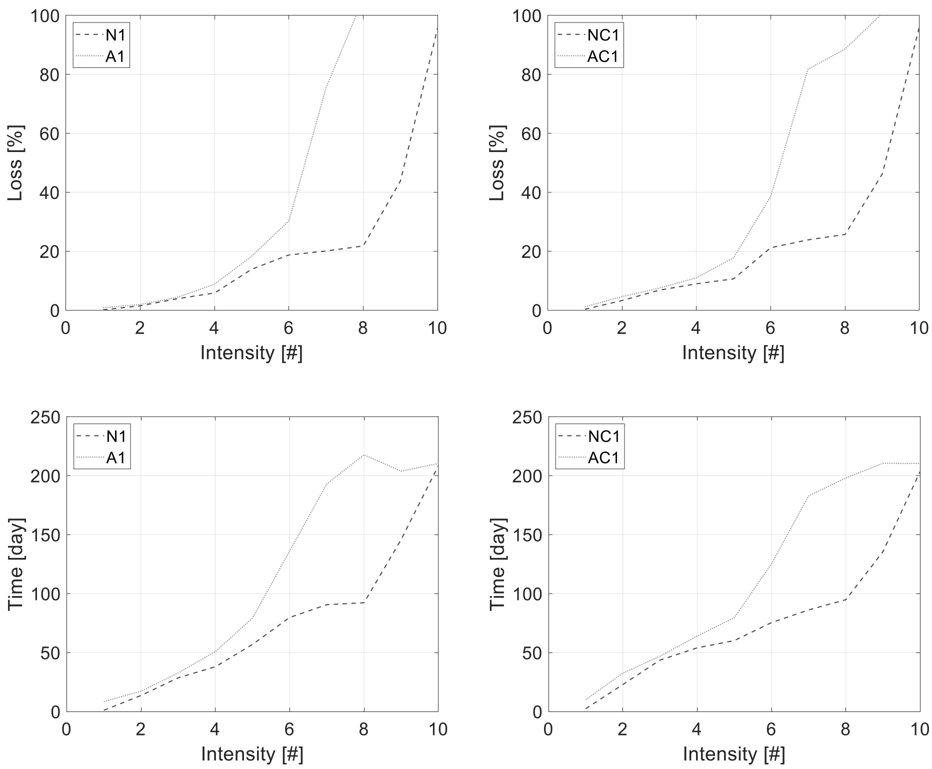

a)

b)

Figure 14 Normalized losses and recovery time for the case of Napoli and L'Aquila.

Figure 15 shows the expected annual loss (EAL) both in terms of cost and recovery time. Again, it is interesting to note how a complete model of the cladding system leads to an increase in terms of both cost and repair time. Such model strategy allows for a more accurate prediction of the non-structural element damage and, consequently, economic losses; despite a low economic value is associated with the repair of non-structural elements, their failure for lower intensity levels is responsible for a high contribution to EAL. It appears reasonable that, given the structural safety as a mandatory condition, the damage to non-structural elements such as the cladding system must be reduced or avoided to effectively reduce the seismic losses in an existing precast structure. Therefore, considering for instance an incremental rehabilitation approach (FEMA-420, Labò et al. 2017), two retrofit steps could be foreseen: first, a minimum intervention to guarantee the life safety at the design basis earthquake (low probability earthquake); then a retrofit intervention to reduce damages on non-structural elements in the case of high probability earthquakes therefore reducing the expected annual losses. Finally, it is worth noting that the modelling strategies proposed may also be adopted in future research for the assessment of the structural behaviour of reference buildings in case of aftershocks (Poiani et al. 2020). An aftershock may lead to an increase in the damage pattern especially in the case of the loss of the support of the structural elements such as in the presence of friction connections (Labò et al. 2022).

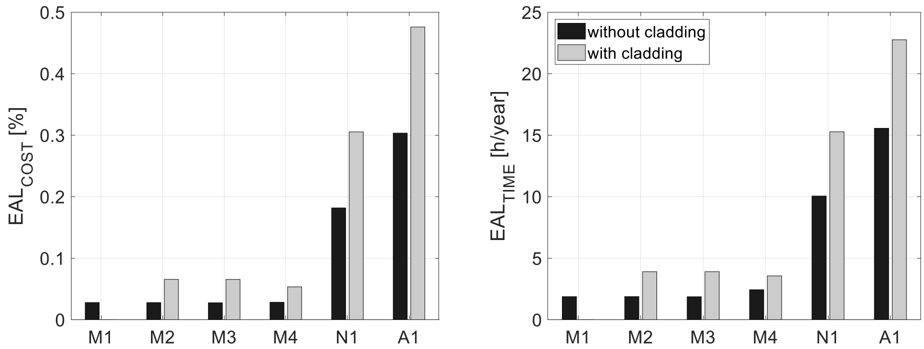

Figure 15 Expected annual losses in terms of cost and recovery time for each model with and without the complete modelling of the cladding panels.

6. Conclusions

The paper investigated the influence of finite element modelling choices on the seismic risk evaluation of precast industrial buildings. A reference case study built in the 1980s in Emilia Romagna (non-seismic area at the time) was supposed located in three different sites with increasing seismic hazard (i.e., Milano, Napoli, and L'Aquila); the original structural details were revised according to the DM 108/86 and a re-design was carried out for the building supposed located in areas classified as seismic at the time of construction.

A sensitivity analysis was carried out to evaluate the influence of the finite element modelling choices; in particular, different hypotheses were made on the roof element boundary conditions (i.e., modelling of mutual contacts), on the diaphragm behaviour of the roof, and on the beam-column connections. Moreover, further considerations were made on the influence of a complete modelling of the cladding panels.

Two modelling strategies for the column reinforced concrete forks were investigated to account for the interaction with the out-of-plane movements of the main girder and its possible overturning. In the first model, rigid elements and compression-only springs were used to model the rocking behaviour of the beam; in the second model, a flexural plastic hinge was introduced at the base of the main beam. In the latter case, a specific calculation code was introduced in the finite element script to calculate, at each step of the analysis, the nonlinear properties of such plastic hinge accounting for the earthquake vertical component and the possible collapse of the supported roof elements. Among the two models, the second option resulted in a more stable solution.

Multi-stripe analyses were then performed for the risk assessment implementing a specific procedure for the element removal after failure. Despite the buildings were re-designed according with DM 108/86, many cases of collapse were recorded. As for the non-structural elements, the cladding panels were either modelled with their actual connections or just modelled as lumped masses.

The results showed that first, the complete modelling of vertically and horizontally spanning cladding panels did not affect the global collapse performance level of the building, but significantly affected the usability preventing damage performance level. This clearly appears in the case of Milano where the collapse of the cladding panels was not detected without the complete modelling of the panels while an increase in the collapse of these elements occurs already for medium intensity values in the case of a complete modelling of the panels. The cladding panel modelling did not affect the global collapse performance level; however, it is important remembering that the collapse of the cladding panels, despite they are regarded as non-structural elements in the design process, can cause injuries and deaths, and, consequently, it cannot be neglected in the seismic safety assessment and its finite element modelling requires a mindful evaluation.

The second aspect to be highlighted is that the structural collapse was mainly associated with the loss of the support of the roof elements. The column collapse was only observed for high intensity earthquakes while the main girder out-of-plane overturning or the beam-column connection collapse never occurred for the considered case studies. Moreover, it is worth noting that the implemented element removal after its collapse allowed for a better estimation of the real participant mass and stiffness thus leading to a better estimation of the building structural behaviour. Therefore, the provision of a horizontal load transfer mechanism through the strengthening of the connections at the roof level is the main intervention required to increase safety.

Third, as for the direct economic losses and the required recovery time, the complete modelling of the cladding panels led to an important increase in economic losses for medium-low intensity events with non-negligible effects in determining the total losses and the related repair and inactivity time of the building, especially in higher seismicity sites such as Napoli and L'Aquila. Indeed, in the expected annual loss evaluation, despite the economic loss value of the cladding system associated with the low intensity earthquakes is low, it is multiplied by a high occurrence probability of the earthquake thus leading to a high contribution to the expected annual losses. Therefore, given the structural safety as a mandatory condition, to effectively reduce the seismic losses in an existing precast structure, the damage to non-structural elements such as the cladding system must be reduced or avoided.

Finally, the proposed modelling strategies may also be adopted in future research for the evaluation of the structural behaviour in case of aftershocks and to assess the influence of the foundation flexibility.

Acknowledgements

The study was partly funded during the activities of the ReLUIS-DPC and EUCENTRE-DPC 2019– 2021 research programs, funded by the Presidenza del Consiglio dei Ministri—Dipartimento della Protezione Civile (DPC). The opinions and conclusions presented by the authors do not necessarily reflect those of the funding entity.

References

Belleri A. (2017). Displacement based design for precast concrete frames with not-emulative connections. Engineering Structures. 141: 228-240.

Belleri A., Cornali F., Passoni C., Marini A., Riva P. (2018). Evaluation of out-of-plane seismic performance of column-to-column precast concrete cladding panels in one-storey industrial buildings. Earthquake Engineering and Structural Dynamics, 47:397–417.

Belleri A., Labò S. (2021). Displacement-based design of precast hinged portal frames with additional dissipating devices at beam-to-column joints. Bulletin of Earthquake Engineering, 19(12):5161-5190.

Belleri A., Torquati M., Marini A., Riva P. (2016). Horizontal cladding panels: in-plane seismic performance in precast concrete Buildings. Bulletin of Earthquake Engineering, 14:1103–1129.

Belleri A., Riva P. (2012). Seismic performance and retrofit of precast concrete grouted sleeve connections. PCI Journal 57 (1): 97–109.

Belleri A., Cornali F., Passoni C., Marini A., Riva P. (2017). Evaluation of out-of-plane seismic performance of column-to-column precast concrete cladding panels in one-storey industrial buildings. Earthquake Engineering and Structural Dynamics, 47:397-417.

Belleri A., Torquati M., Marini A., Riva P. (2016). Horizontal cladding panels: in-plane seismic performance in precast concrete buildings. Bulletin of Earthquake Engineering, 14:1103-1129.

Belleri A., Torquati M., Riva P., Nascimbene R. (2015). Vulnerability assessment and retrofit solutions of precast industrial structures. Earthquakes and Structures, 8(3):801–820.

Biondini F., Toniolo G. (2009). Probabilistic calibration and experimental validation of the seismic design criteria for one-storey concrete frames. Journal of Earthquake Engineering, 13(4):426-462.

Biondini F., Toniolo G., Tsionis G. (2010), Capacity Design and Seismic Performance of Multi-Story Precast Structures, European Journal of Environmental and Civil Engineering, 14(1):11-28.

Bosio M, Di Salvatore C, Bellotti D, Capacci L, Belleri A, Piccolo V, Cavalieri F, Dal Lago B, Riva P, Magliulo G, Nascimbene R, Biondini F. (2022). Modelling and seismic response analysis of non-residential single-storey existing precast buildings in Italy. Journal of Earthquake Engineering. doi: 10.1080/13632469.2022.2033364.

Bosio M., Belleri A., Riva P., Marini A. (2020). Displacement-Based Simplified Seismic Loss Assessment of Italian Precast Buildings. Journal of Earthquake Engineering 24(sup1):60-81.

Bournas D.A., Negro P., Taucer F.F. (2014). Performance of industrial buildings during the Emilia earthquakes in North-ern Italy and recommendations for their strengthening. Bulletin of Earthquake Engineering, 12(5):2383–2404.

Bressanelli ME., Belleri A., Riva P., Magliulo G., Bellotti D., Dal Lago B. (2019). Effects of modeling assumptions on the evaluation of the local seismic response for RC precast industrial buildings. In 7th International Conference on Computational Methods in Structural Dynamics and Earthquake Engineering Methods in Structural Dynamics and Earthquake Engineering–COMPDYN, Crete, Greece (pp. 24-26).

Bressanelli ME., Bellotti D., Belleri A., Cavalieri F., Riva P., Nascimbene R. (2021). Influence of Modelling Assumptions on the Seismic Risk of Industrial Precast Concrete Structures. Front. Built Environ. 7:629956. doi: 10.3389/fbuil.2021.629956.

Casotto C., Silva V., Crowley H., Nascimbene R., Pinho R. (2015). Seismic fragility of Italian RC precast industrial structures. Engineering Structures, 94: 122–36.

CEN (2004). Eurocode 8: Design of structures for earthquake resistance - Part 1: General rules, seismic actions and rules for buildings. European Standard, Brussels, Belgium.

Clementi F., Scalbi A., Lenci S. (2016). Seismic performance of precast reinforced concrete buildings with dowel pin connections. J. Building Eng. 7, 224-238.

CNR 10025 (1984). Prefabbricazione e strutture prefabbricate. Consiglio Nazionale delle Ricerche 1984, n°10025 (in Italian).

Colombo A., Negro P., Toniolo G., Lamperti M. (2016). Design guidelines for precast structures with cladding panels. JRC Technical report, ISBN 978-92-79-58534-0.

Dal Lago B., Toniolo G., Felicetti R., Lamperti Tornaghi M. (2017). End support connection of precast roof elements by bolted steel angles. Structural Concrete, 18(5):755-767.

Dal Lago B., Toniolo G., Lamperti Tornaghi M. (2016). Influence of different mechanical column-foundation connection devices on the seismic behaviour of precast structures. Bulletin of Earthquake Engineering, 14(12):3485–3508.

De Stefani L., Scotta R. (2022). Seismic behavior of precast buildings with dissipative connections. advances in seismic performance and risk estimation of precast concrete buildings. Front. Built Environ. Doi: 10.3389/fbuil.2021.639777.

Decreto Ministeriale n. 108 (1986). Norme tecniche relative alle costruzioni antisismiche. In Italian.

Demartino C., Vanzi I., Monti G., Sulpizio C. (2018). Precast industrial buildings in Southern Europe: loss of support at frictional beam-to-column connections under seismic actions. Bulletin of Earthquake Engineering, 16(1):259-294.

Ercolino M., Magliulo G., Manfredi G. (2016). Failure of a precast RC building due to Emilia-Romagna earthquakes. Engineering Structures, 118:262-273.

FEMA P-58-3.1 [2016]. Seismic Performance Assessment of Buildings Volume 3—Performance 567 Assessment Calculation Tool (PACT) Version 2.9.65, Applied Technology Council

Gajera K, Dal Lago B, Capacci L, Biondini F. (2021). Multi-stripe seismic assessment of precast industrial buildings with cladding panels. Front. Built Environ. 7:631360. Doi: 10.3389/fbuil.2021.631360.

Ibarra L., Medina R., Krawinkler H. (2005). Hysteretic Models that Incorporate Strength and Stiffness Deterioration. Earthquake Engineering and Structural Dynamics 34:1489-1511.

Iervolino I., Spillatura A., Bazzurro P. (2018). Seismic reliability of code-conforming Italian buildings. Journal of Earthquake Engineering 22 (sup2): 5–27.

Iervolino I., Baraschino R., Spillatura A. (2022). Evolution of seismic reliability of code-conforming Italian buildings. Journal of Earthquake Engineering, doi: 10.1080/13632469.2022.2087801

Kremmyda G. D., Fahjan Y. M., Tsoukantas S. G. (2014). Nonlinear FE analysis of precast RC pinned beam-to-column connections under monotonic and cyclic shear loading. Bulletin of Earthquake Engineering, 12:1615–1638.

Labò S., Eteme M., Marini A., Belleri A. (2022). Loss of support assessment for precast portal frames with friction connections and masonry infills. Bulletin of Earthquake Engineering, doi: 10.1007/s10518-022-01489-7

Magliulo G., Bellotti D., Cimmino M., Nascimbene R. (2018). Modeling and Seismic Response Analysis of RC Precast Italian Code-Conforming Buildings. Journal of Earthquake Engineering, 22(sup2):140-167.

Magliulo G., Capozzi V., Fabbrocino G., Manfredi G. (2011). Neoprene–concrete friction relationships for seismic assessment of existing precast buildings. Engineering Structures 33:532–358.

Magliulo G., Di Salvatore C., Ercolino M. (2021). Modeling of the Beam-To-Column Dowel Connection for a Single-Story RC Precast Building. Front. Built Environ. 7: 627546. Doi: 10.3389/fbuil.2021.627546.

Magliulo G., Ercolino M., Cimmino M., Capozzi V., Manfredi G. (2014). FEM analysis of the strength of RC beam-to-column dowel connections under monotonic actions. Construct Build Mater. 69:271-284.

Magliulo G., Ercolino M., Petrone C., Coppola O., Manfredi G. (2014). The Emilia earthquake: seismic performance of precast reinforced concrete buildings. Earthquake Spectra, 30(2):891–912.

McKenna F., Fenves G. (2001). The OpenSees Command Language Manual: version 1.2- Pacific Earthquake Engineering Center, Univ. of Calif., Berkeley.

Menichini G., Del Monte E., Orlando M., Vignoli A. (2020). Out-of-plane capacity of cladding panel-to-structure connections in one-story R/C precast structures. Bulletin of Earthquake Engineering, 18:6849–6882.

Metelli G., Beschi C., Riva P. (2011). Cyclic behaviour of a column to foundation joint for concrete precast structures. Eur J Environ Civ Eng. 15(9):1297-1318.

Minghini F., Ongaretto E., Ligabue V., Savoia M., Tullini N. (2016). Observational failure analysis of precast buildings after the 2012 Emilia earthquakes. Earthquakes and Structures 11(2):327–46.

Nastri E., Vergato M., Latour M. (2017). Performance evaluation of a seismic retrofitted R.C. precast industrial building. Earthquakes and Structures 12(1). doi: 10.12989/eas.2017.12.1.013.

Osanai Y., Watanabe F., Okamoto S. (1996). Stress transfer mechanism of socket base connections with precast concrete columns. ACI Struct J. 93(3):266-276.

Palanci M., Senel S.M., Kalkan A. (2017). Assessment of one story existing precast industrial buildings in Turkey based on fragility curves. Bull. Earthq. Eng. 15(1): 271–289.

Rodrigues H., Vitorino H., Batalha N., Sousa R., Fernandes P., Varum H. (2021). Influence of Beam-to-Column Connections in the Seismic Performance of Precast Concrete Industrial Facilities. Structural Engineering International, doi: 10.1080/10168664.2021.1920082.

Poiani M., Gazzani V., Clementi F., Lenci S. (2020). Aftershock fragility assessment of Italian cast–in–place RC industrial structures with precast vaults. Journal of Building Engineering, 29, 101206, doi: 10.1016/j.jobe.2020.101206.

Savoia M., Mazzotti C., Buratti N., Ferracuti B., Bovo M., Ligabue V. (2012). Damages and collapses in industrial precast buildings after the Emilia earthquake. Ingegneria Sismica, 29:120–131.

Scotta R., De Stefani L., Vitaliani R. (2015). Passive control of precast building response using cladding panels as dissipative shear walls. Bulletin of Earthquake Engineering, 13:3527–3552.

Sousa R., Batalha N., Silva V., Rodrigues H. (2020). Seismic fragility functions for Portuguese RC precast buildings. Bull Earthquake Eng. 19:6573-6590.

Toniolo G., Colombo A. (2012). Precast concrete structures: the lessons learned from the L'Aquila earthquake. Structural Concrete, 13(2):73-83.

Torquati M., Belleri A., Riva P. (2018). Displacement-Based Seismic Assessment for Precast Concrete Frames with Non-Emulative Connections. Journal of Earthquake Engineering. 24(10): 1624-1651.

Zoubek B., Fischinger M., Isakovic T. (2016). Cyclic response of hammer-head strap cladding-to-structure connections used in RC precast building. Engineering Structures, 119:135–148.

Zoubek B., Fahjan Y., Fischinger M., Isakovic T. (2014). Nonlinear finite element modelling of centric dowel connections in precast buildings. Eng. structures 14(4):463–477.

Zoubek B., Fischinger M., Isakovic T. (2015). Estimation of the cyclic capacity of beam-to-column dowel connections in precast industrial buildings. Bulletin of Earthquake Engineering, 13(7):2145–2168.